Prepared for submission to JCAP

Testing for New Physics: Neutrinos and the Primordial Power Spectrum

Nicolas Canac,[a] **Grigor Aslanyan,**[b] **Kevork N. Abazajian,**[a] **Richard Easther,**[c] **and Layne C. Price**[d]

[a]Department of Physics, University of California at Irvine, Irvine, CA 92697

[b]Berkeley Center for Cosmological Physics, University of California, Berkeley, CA 94720, USA

[c]Department of Physics, University of Auckland, Private Bag 92019, Auckland, New Zealand

[d]McWilliams Center for Cosmology, Department of Physics, Carnegie Mellon University, Pittsburgh, PA 15213, USA

E-mail: ncanac@uci.edu, aslanyan@berkeley.edu, kevork@uci.edu, r.easther@auckland.ac.nz, laynep@andrew.cmu.edu

Abstract. We test the sensitivity of neutrino parameter constraints from combinations of CMB and LSS data sets to the assumed form of the primordial power spectrum (PPS) using Bayesian model selection. Significantly, none of the tested combinations, including recent high-precision local measurements of H_0 and cluster abundances, indicate a signal for massive neutrinos or extra relativistic degrees of freedom. For PPS models with a large, but fixed number of degrees of freedom, neutrino parameter constraints do not change significantly if the location of any features in the PPS are allowed to vary, although neutrino constraints are more sensitive to PPS features if they are known *a priori* to exist at fixed intervals in $\log k$. Although there is no support for a non-standard neutrino sector from constraints on both neutrino mass and relativistic energy density, we see surprisingly strong evidence for features in the PPS when it is constrained with data from *Planck* 2015, SZ cluster counts, and recent high-precision local measurements of H_0. Conversely combining *Planck* with matter power spectrum and BAO measurements yields a much weaker constraint. Given that this result is sensitive to the choice of data this tension between SZ cluster counts, *Planck* and H_0 measurements is likely an indication of unmodeled systematic bias that mimics PPS features, rather than new physics in the PPS or neutrino sector.

ArXiv ePrint: 1606.03057

arXiv:1606.03057v2 [astro-ph.CO] 20 Sep 2016

Contents

1 Introduction **1**

2 Method **3**
- 2.1 Non-power-law primordial power spectrum 3
- 2.2 Model, priors, and Bayesian evidence 4
- 2.3 Data sets 8

3 Results and Discussion **10**

4 Conclusion **15**

1 Introduction

Cosmological observations have emerged as a stringent constraint on the total mass of neutrinos. The total neutrino mass makes a subtle contribution to cosmic microwave background (CMB) anisotropies and has a more substantial impact on the late time matter power spectrum measured via clustering observations. The CMB is sensitive to neutrino mass and effective neutrino number via the alteration of matter-radiation equality leading up to the decoupling of the CMB, and the alteration of the evolution of the neutrino anisotropic stress-energy tensor. Extra relativistic energy density modifies the acoustic peak scale to the photon-damping scale, making the CMB a sensitive measure of relativistic energy density above the photon density, often parameterized as $N_{\rm eff} \equiv (\rho_{\rm rad} - \rho_\gamma)/\rho_\nu$, where $\rho_{\rm rad}$, ρ_γ, and ρ_ν are the total energy density in relativistic species, photons, and active neutrinos, respectively.

Cosmological large scale structure (LSS) is sensitive to the presence of massive neutrinos and effective neutrino number $N_{\rm eff}$. Baryon acoustic oscillations (BAO) are affected by the change of matter-radiation equality and commensurate change in expansion history. Measurements of LSS clustering, such as the power spectrum of galaxies, are a sensitive probe of neutrino properties as clustering is suppressed below the neutrino free streaming scale via a combination of the relativistic behavior of neutrinos at early times and their free-streaming suppression of late time growth. The sensitivity of galaxy clustering was highlighted some time ago (*e.g.*, [1]), and future probes can achieve very high precision (For a recent review, see Ref. [2]).

When combined with LSS observables, the complementary role of the CMB removes degeneracies with other cosmological parameters allowing high-precision determinations of their values. For example, the scalar perturbation amplitude A_s, tilt n_s and matter density Ω_m are each, to different degrees, degenerate with $\sum m_\nu$, but are determined to percent-level precision from Planck's 2015 CMB analysis [3]. In single-parameter extensions of ΛCDM in which the sum of neutrino masses is a free parameter, the resulting constraints are an order of magnitude tighter than current kinematic laboratory constraints: $\sum m_\nu < 0.23$ eV (95%) from Planck 2015 (TT, lowP, lensing, BAO, JLA, H_0) [3], versus $\sum m_\nu \lesssim 6$ eV from ^{3}H β decay plus oscillations [4]. The latest Planck data (TT, TE, EE, SimLow, lensing) [5] yields $\sum m_\nu < 0.14$ eV(95%), but the HFI likelihood codes are not yet public. Here the sum of neutrino masses is defined as the sum of the individual mass eigenstates $\Sigma m_\nu \equiv m_1 + m_2 + m_3$

and does not depend on their hierarchical ordering beyond the mass degeneracy scale where $m_1 \approx m_2 \approx m_3$.

In the past several years, there have been indications of tension between local probes of cosmological structure and expansion and values obtained from analyses of CMB data. The tension comes in two regards: first, the CMB-parameter inferred local Hubble expansion rate at present, H_0, is lower than precise local measures; and second, the amplitude of scalar perturbations inferred from the CMB is higher than that from more local measures. The combination of the CMB with these local probes are often referred to as tension data sets and we adopt that here. These tension data sets include analyses of combinations of CMB and H_0 data with SPT SZ clusters by Hou et al. [6], and combinations of CMB data with cosmic shear lensing data from CFHTLenS also indicated a nonzero neutrino mass [7], as well as data from the Baryon Oscillation Spectroscopic Survey (BOSS) constant mass (CMASS) luminous red galaxy sample [8]. With such combinations of data sets between local and high redshift cosmology measures, there were a number of combinations that indicated degenerate neutrino masses or extra relativistic energy density could relieve this tension [9–14]. Whether the evidence for strong tension and new neutrino physics from the low redshift measures is definitive has been called into question by several papers [3, 15, 16]. For example, weak lensing systematics has been shown to alleviate tension in that data set [17]. Generally, the low redshift data indicates a lower amplitude of fluctuations on relatively small scales, parameterized as σ_8, the rms over-density of fluctuations smoothed with a spherical window function of $8h^{-1}$ Mpc. Although there exist several different cluster abundance samples that indicate tension with the CMB [18–21], we employ, as a representative measure, constraints on σ_8 vs Ω_m from Planck SZ Clusters, as described below [11, 19]. Additional tension is indicated in recent high-precision measures of the local expansion rate H_0, which has been proposed to potentially indicate extra relativistic energy density ($N_{\rm eff} > 3$) [22]. Importantly, the tension between low and high redshift perturbation amplitude is at least partially alleviated in new polarization measures of reionization that reduce the inferred scalar amplitude [5]. In summary, a number of tension data sets have suggested non-standard relativistic energy or non-trivial neutrino mass, but the results are inconclusive, nor are necessarily mutually consistent. Such tension could very well indicate new physics and is why we include it in our investigation.

Cosmological neutrino mass measurements are approaching the sensitivity needed to detect the minimal value of $\sum m_\nu \approx$ 60 meV derived from the mass-splittings in the neutrino sector inferred from neutrino oscillations. However, reliably achieving this sensitivity requires a careful analysis of the assumptions and model dependencies underlying cosmological constraints. Several cosmological model dependencies are discussed in, *e.g.* Ref. [23]. In particular, the effects of massive neutrinos on large scale structure can be degenerate with deviations from smoothness in the primordial power spectrum (PPS). In particular, given a fine-tuned PPS, CMB data can mimic a zero neutrino mass universe even if the neutrino density is large [24]. It is therefore important to test the dependence of neutrino parameter constraints on the assumed shape of the PPS. The consequences of a non-trivial PPS for neutrino constraints were previously analyseds in Refs. [25–27]. Those analyses consider a PPS in which features and/or discontinuities were located at specified wavenumbers. In this paper, we consider more general scenarios in which the features locations are constrained by the data, employing the Bayesian model selection methods of Ref [28, 29] to determine whether the improved fit justified the increased complexity of the model.

Separately, we go beyond previous work by exploring tension between SZ cluster abun-

dances and recent high-precision measures of H_0 in the "local" universe. We combine the 2015 Planck results [3], large-volume galaxy survey LSS data from the clustering of Luminous Red Galaxies from the Sloan Digital Sky Survey [30], and the WiggleZ Dark Energy Survey [31]. We also use the most recent measures of the Baryon Acoustic Oscillation (BAO) scale from the six-degree-Field Galaxy Survey (6dFGS) [32], from the SDSS Main Galaxy Sample (SDSS-MGS) [33], and from the Baryon Oscillation Spectroscopic Survey data release 11 (BOSS DR11), from both the LOWZ and CMASS samples [34], which provide robust complementary constraints on the cosmological parameters, including neutrinos. In order to claim strong evidence for new physics from the combined analysis of these tension data sets, it is necessary that different probes of the same cosmological signals, *e.g.*, expansion history or growth rate, provide comparable statistical evidences for the same extensions to ΛCDM. In contrast, if different models are favored with wildly variable confidences, then this provides some evidence for unmodeled bias in the probes themselves. In light of this, here we aim to test for the evidence of novel signals in the neutrino sector or the primordial spectrum.

2 Method

In this section we begin by describing the cosmological models we analyze, along with the "knot-spline" algorithm used to reconstruct the PPS. We also give our priors for the parameters in our models and discuss the use of Bayesian evidence and posterior probabilities in model selection and parameter estimation.

The likelihood calculations and PPS reconstruction are performed using the publicly available code CosmoMC++ [35]. The CMB power spectra and matter power spectrum are calculated using the CLASS package [36, 37]. The parameter space sampling and Bayesian evidence calculation is implemented with the publicly available multimodal nested sampling code MultiNest [38–40]. Finally, the resulting chains are analyzed and plotted using the GetDist Python package.

2.1 Non-power-law primordial power spectrum

Our goal is to examine how constraints on neutrino parameters change when we relax the assumption that the PPS has a simple power-law form. In particular, we want to test the sensitivity of neutrino parameters to the shape of the PPS. Our approach to reconstructing the PPS is a variation of the "knot-spline" method described in [28, 29, 41]. Similar methods implementing a free-form primordial spectrum are given in Refs. [25, 27, 42–51].

The algorithm is summarized as follows:

1. Fix $k_{\rm min} = 10^{-6}\,{\rm Mpc}^{-1}$ and $k_{\rm max} = 10.0\,{\rm Mpc}^{-1}$, but allow their amplitudes $A_{\rm min}$ and $A_{\rm max}$ to vary.

2. Add n knots with uniform priors on $\log k$, in the range $\log k_{\rm min} < \log k_i < \log k_{\rm max}$ and a uniform prior on A_i, in the range $-2 < A_i < 4$, where $A_i \equiv \log(10^{10}\Delta^2_\zeta(k_i))$, where Δ^2_ζ is the dimensionless PPS of curvature perturbations and $i = 1, 2, ..., n$. The knots are ordered so that $k_{i-1} \leq k_i$, and the number of knots n is varied between 1 and 5.

3. Interpolate between the endpoints and the n ordered knots using a linear spline. The interpolation is performed in logarithmic space for both k and Δ^2_ζ.

We adopt uniform priors for the locations of knots in $\log k$ and their amplitudes. Knots with arbitrary locations in k-space are able to capture both local, step-like feature, more

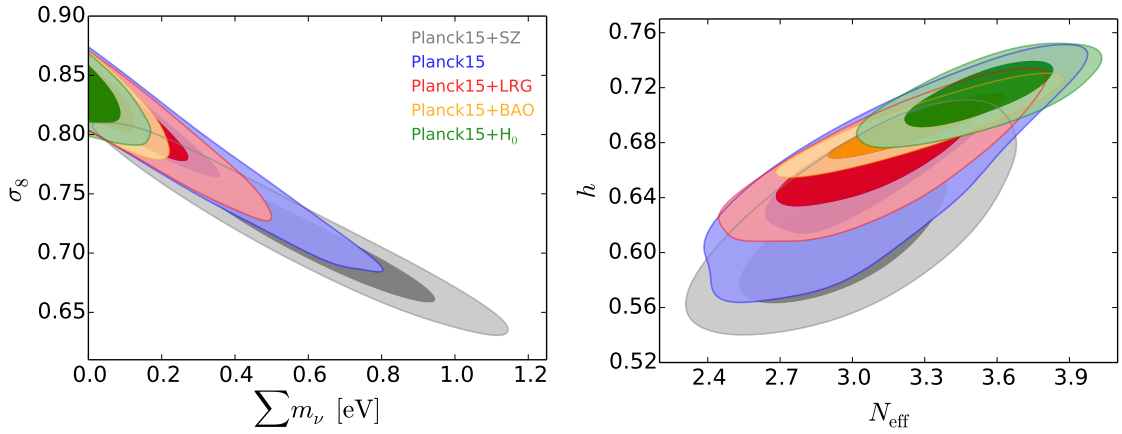

Figure 1. *(Left)* The two-dimensional posterior distribution showing the 68% and 95% CI allowed regions in the $\sigma_8 - \sum m_\nu$ plane for 0 knots and $\sum m_\nu$ free for various combinations of data. *(Right)* The same but for $N_{\rm eff}$ in the $h - N_{\rm eff}$ plane.

gradual changes like a large-scale exponential suppression, or a spectrum with a sharp cutoff. With no knots, the PPS is specified by two parameters, the amplitudes of the endpoints $k_{\rm min}$ and $k_{\rm max}$. In this case, the PPS is equivalent to the standard power-law PPS in ΛCDM, providing for an easy comparison between the two models. Each additional knot yields two degrees of freedom corresponding to the location of the knot k_i and its amplitude A_i. In total, $2n + 2$ free parameters specify the PPS model, where n is the number of knots. Allowing the knot location to vary provides some basic protection against the look-elsewhere effect or multiple comparisons problem, since the knot is free to move over the global range of k, in contrast to reconstructions in which the knot locations are fixed. The broad ranges from which $k_{\rm knot}$ and $A_{\rm knot}$ are drawn allow for possible features at any measurable scale.

2.2 Model, priors, and Bayesian evidence

We choose uniform priors for all cosmological variables, including the usual parameters $\Omega_b h^2$, $\Omega_c h^2$, h, and τ, the sum of the neutrino masses $\sum m_\nu$ and the effective number of relativistic degrees of freedom $N_{\rm eff}$. As explained above, the knot-spline specification of the PPS has two parameters associated with each knot, $\log_{10} k_{\rm knot}$ and $\log(10^{10}\Delta^2_{\rm knot})$, and two additional parameters describing the amplitudes of the fixed endpoints. The ranges for these priors are shown in Table 1.

To evaluate the statistical significance of a model $\mathcal{M}$, we use the posterior probability $P(\mathcal{M}\,|\,\text{Data})$. For two models $\mathcal{M}_i$ and $\mathcal{M}_j$ with the same prior probability, the evidence ratio or Bayes factor is given by

$$\frac{Z_i(D)}{Z_j(D)} = \frac{P(\text{Data}\,|\,\mathcal{M}_i)}{P(\text{Data}\,|\,\mathcal{M}_j)}\,, \tag{2.1}$$

where the Bayesian evidence or marginalized likelihood is

$$Z_i(D) \equiv P(\text{Data}\,|\,\mathcal{M}_i) = \int P(\theta\,|\,\mathcal{M}_i)\,\mathcal{L}(\text{Data}\,|\,\theta) d\theta \tag{2.2}$$

for the model parameters θ. Here, $\mathcal{L}(\text{Data}\,|\,\theta)$ is the data-likelihood and $P(\theta\,|\,\mathcal{M}_i)$ is the parameter prior probability. When the prior probabilities for the models are equal (as is

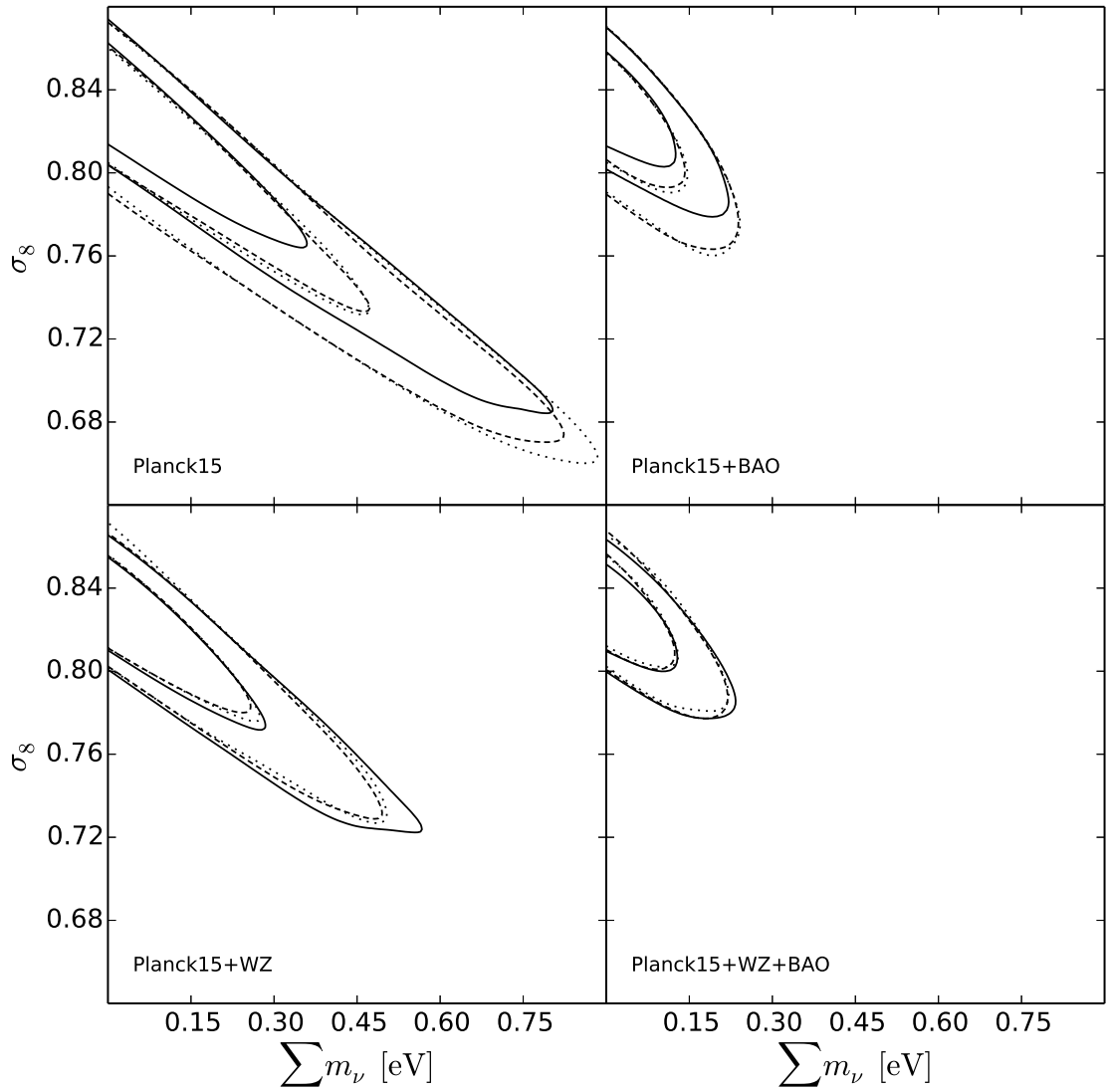

Figure 2. Two-dimensional posterior distributions in the $\sigma_8 - \sum m_\nu$ plane for 0 knots (solid line), 1 knot (dashed line), and 2 knots (dotted line) for various combinations of data sets. Models with more than 2 knots do not differ significantly from the $n = 2$ case and are not displayed.

common convention) the Bayes' factor directly measures the posterior model odds. We allow for a wide range of values when specifying potential features in the PPS at fixed number of degrees of freedom in our parameterization. In general, the integral in equation (2.2) is numerically challenging but can be computed using multimodal nested sampling.

It is more convenient to use the logarithm of the Bayes factor:

$$\Delta \ln Z \equiv \ln \frac{Z_i(D)}{Z_j(D)} \,. \tag{2.3}$$

Evidence ratios can be interpreted qualitatively using the Jeffreys' scale [52] or a more conservative "cosmology scale" [53], summarized in Table 2. Bayesian model selection yields a global estimate of how well a model fits the data by integrating over the entirety of parameter

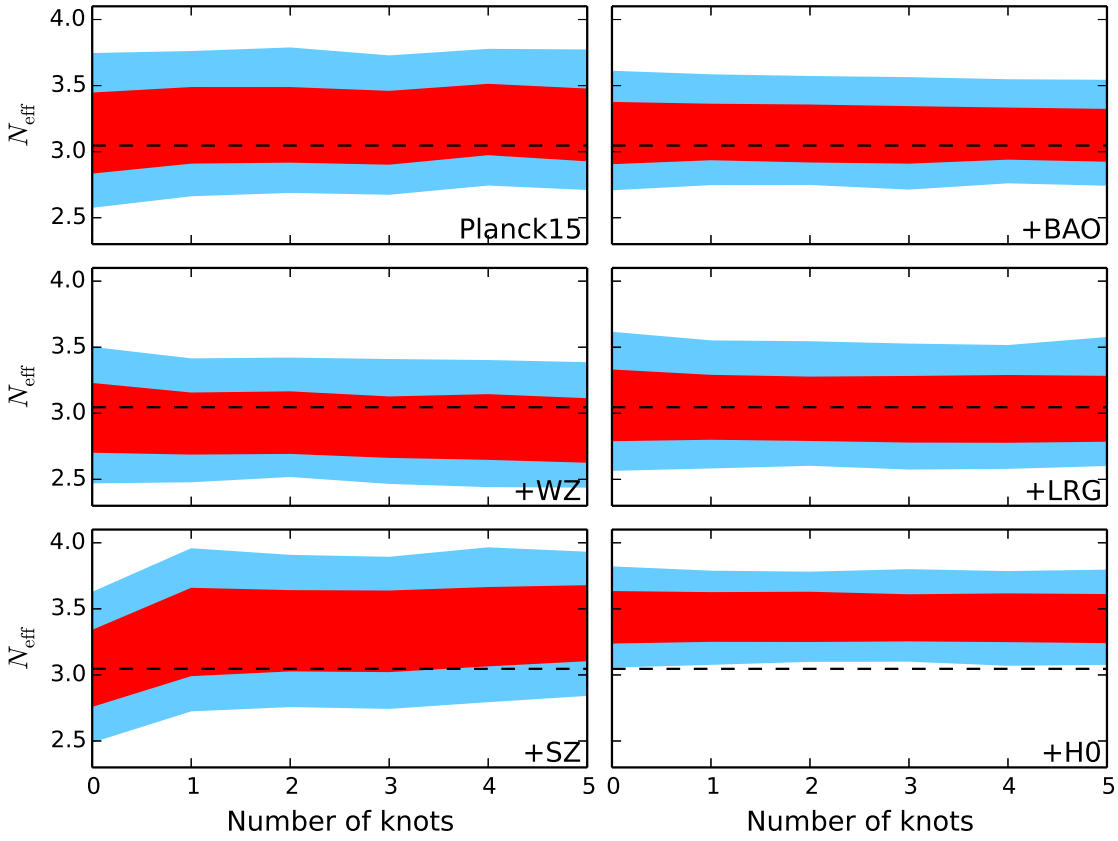

Figure 3. 68% and 95% CI constraints on $N_{\rm eff}$ for models with $N_{\rm eff}$ allowed to vary and PPS reconstruction with knot location free. The data sets used are indicated in each panel (Planck15 is implicitly included in each panel).

Parameter	Prior	Parameter	Prior
$\Omega_b h^2$	$[0.020, 0.025]$	$\sum m_\nu$	$[0.001, 3.0]$
$\Omega_c h^2$	$[0.10, 0.14]$	$N_{\rm eff}$	$[2.0, 5.0]$
h	$[0.55, 0.80]$	$\log_{10} k_{\rm knot}$	$[-6, 1]$
τ	$[0.04, 0.12]$	$\log(10^{10}\Delta^2_{\rm knot})$	$[-2, 4]$

Table 1. Ranges for uniform priors for cosmological parameters.

space and the Bayes factor penalizes those complex models with many free parameters that yield a high value for the likelihood only within some small sub-region of the overall parameter space. A model with more parameters must thus yield a significant improvement in likelihood over a sufficiently large volume of parameter space in order to yield posterior odds that support the more complex model.

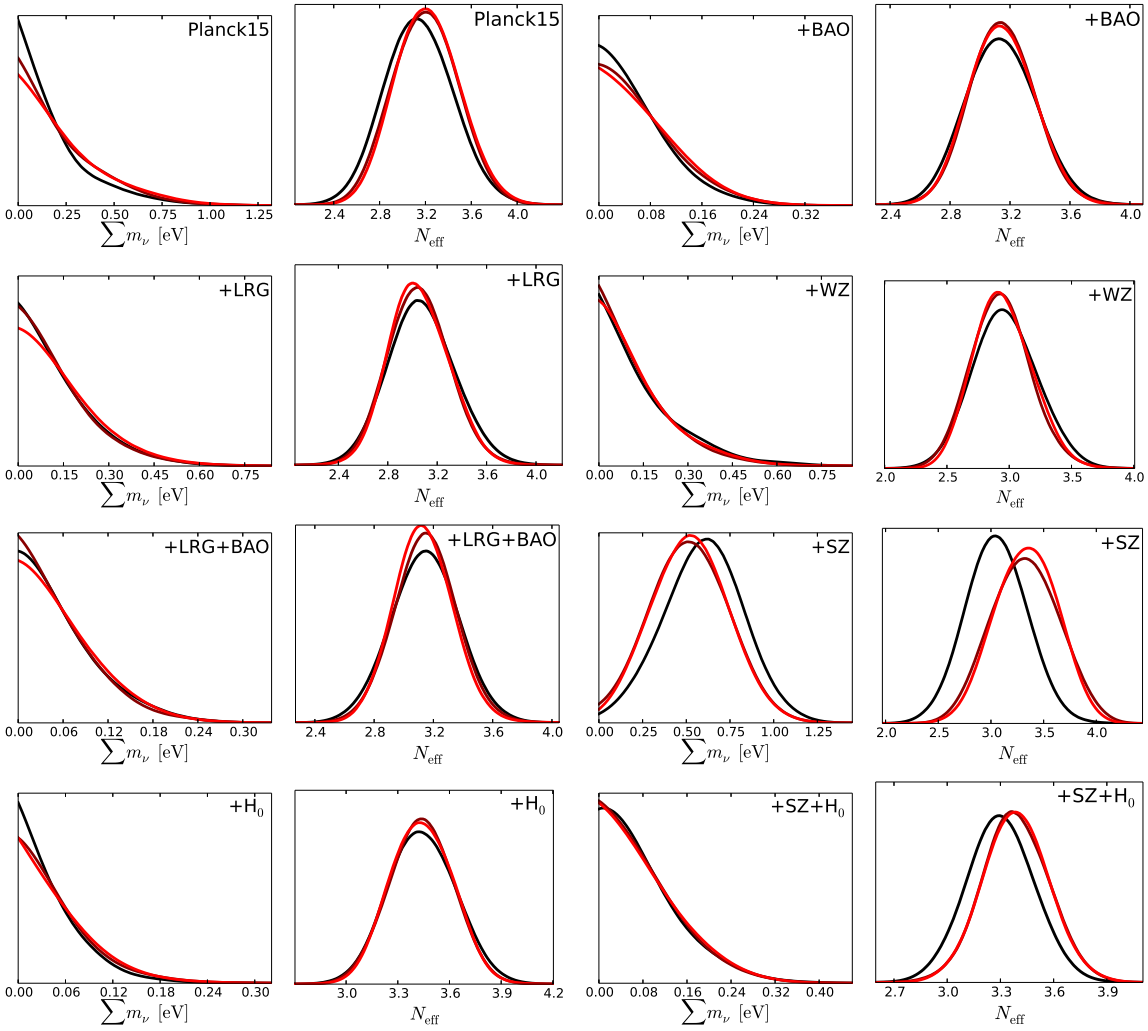

Figure 4. One-dimensional posterior distributions for $\sum m_\nu$ and $N_{\rm eff}$. The colors of the contours from darkest to lightest indicate increasing number of knots in the PPS from 0 to 2 knots. Higher numbers of knots do not lead to significant changes. All cases shown are for models where the knot location in k is a free parameter.

log (*Posterior Odds*)	Jeffreys Scale	Cosmology Scale
0.0 to 1.0	Not worth more than a bare mention	
1.0 to 2.5	Substantial	Weak
2.5 to 5.0	Strong	Significant
> 5	Decisive	Strong

Table 2. Rough guideline for Bayesian evidence interpretation with the Jeffreys scale [52] and the more conservative "cosmology scale" from Ref. [53].

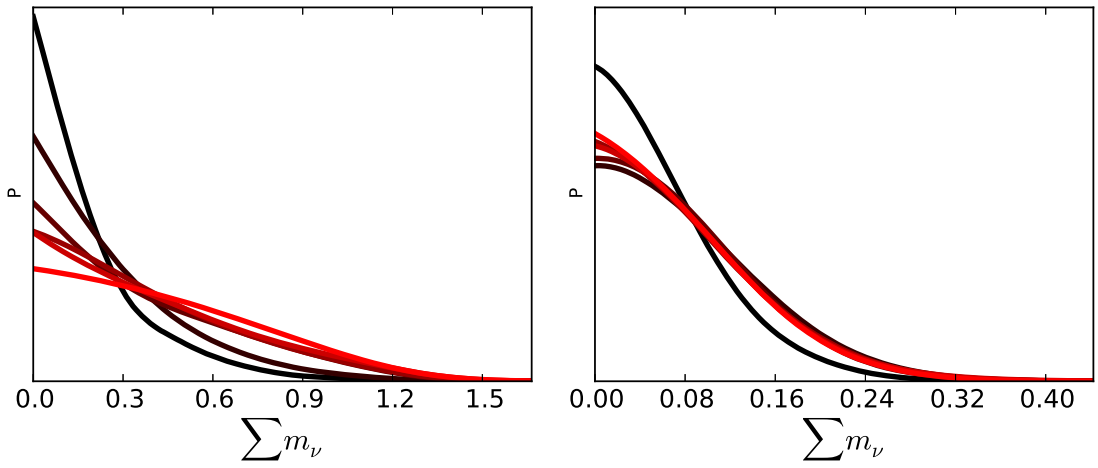

Figure 5. One-dimensional posterior distributions for $\sum m_\nu$ for (*left*) Planck15 only and (*right*) Planck15+BAO for the case of fixed knots. The color of line from dark to light represents increasing numbers of knots from 0 to 10 in intervals of 2.

Data	No knots	1 knot	2 knots	3 knots	4 knots	5 knots
Planck15	0.63	0.66	0.71	0.64	0.71	0.67
Planck15+BAO	0.18	0.19	0.19	0.18	0.20	0.24
Planck15+WZ	0.44	0.40	0.40	0.39	0.43	0.37
Planck15+LRG	0.40	0.40	0.43	0.39	0.39	0.38
Planck15+H_0	0.13	0.15	0.15	0.18	0.15	0.18
Planck15+WZ+BAO	0.18	0.18	0.18	0.17	0.17	0.17
Planck15+LRG+BAO	0.17	0.16	0.17	0.17	0.16	0.22
P15+LRG+BAO+H_0	0.14	0.13	0.13	0.16	0.17	0.13
Planck15+SZ+H_0	0.23	0.23	0.23	0.24	0.23	0.24
Planck15+SZ	$0.60^{+0.22}_{-0.23}$	$0.52^{+0.22}_{-0.24}$	$0.52^{+0.22}_{-0.23}$	$0.53^{+0.21}_{-0.23}$	$0.49^{+0.20}_{-0.23}$	$0.49^{+0.20}_{-0.22}$

Table 3. 95% CI upper limits on $\sum m_\nu$ in eV for various combinations of data and numbers of knots for the model cases where $\sum m_\nu$ is allowed to vary in addition to the standard cosmological parameters and knots with k and amplitude freedom in position. The 68% CI constraints are also shown in the bottom row for the tension data set.

2.3 Data sets

We use measurements of the CMB, the matter power spectrum, BAO, SZ cluster counts, and Hubble constant H_0, which we describe in detail below. Likelihood modules for each of these data sets have been written for use with Cosmo++.

Cosmic Microwave Background.— For all the runs performed in this analysis, we use the CMB measurements from the Planck 2015 data release [54]. Although better constraints

Data	No knots	1 knot	2 knots	3 knots	4 knots	5 knots
Planck15	$3.14^{+0.31}_{-0.31}$	$3.20^{+0.29}_{-0.29}$	$3.22^{+0.27}_{-0.30}$	$3.19^{+0.27}_{-0.29}$	$3.25^{+0.26}_{-0.28}$	$3.22^{+0.26}_{-0.29}$
Planck15+BAO	$3.14^{+0.24}_{-0.24}$	$3.15^{+0.21}_{-0.21}$	$3.15^{+0.21}_{-0.23}$	$3.14^{+0.21}_{-0.23}$	$3.14^{+0.20}_{-0.20}$	$3.14^{+0.19}_{-0.21}$
Planck15+WZ	$2.97^{+0.26}_{-0.27}$	$2.93^{+0.23}_{-0.24}$	$2.95^{+0.22}_{-0.25}$	$2.91^{+0.22}_{-0.25}$	$2.91^{+0.23}_{-0.27}$	$2.90^{+0.22}_{-0.27}$
Planck15+LRG	$3.07^{+0.26}_{-0.28}$	$3.05^{+0.24}_{-0.25}$	$3.05^{+0.23}_{-0.26}$	$3.04^{+0.24}_{-0.26}$	$3.04^{+0.25}_{-0.26}$	$3.05^{+0.23}_{-0.27}$
Planck15+H_0	$3.44^{+0.19}_{-0.20}$	$3.44^{+0.19}_{-0.19}$	$3.44^{+0.19}_{-0.19}$	$3.44^{+0.17}_{-0.19}$	$3.43^{+0.19}_{-0.18}$	$3.43^{+0.19}_{-0.18}$
Planck15+WZ+BAO	$3.01^{+0.21}_{-0.20}$	$3.02^{+0.19}_{-0.22}$	$3.01^{+0.18}_{-0.19}$	$3.00^{+0.19}_{-0.19}$	$3.01^{+0.18}_{-0.18}$	$3.01^{+0.19}_{-0.19}$
Planck15+LRG+BAO	$3.14^{+0.23}_{-0.23}$	$3.15^{+0.20}_{-0.21}$	$3.13^{+0.20}_{-0.20}$	$3.15^{+0.21}_{-0.22}$	$3.13^{+0.20}_{-0.19}$	$3.14^{+0.21}_{-0.22}$
P15+LRG+BAO+H_0	$3.36^{+0.19}_{-0.19}$	$3.36^{+0.17}_{-0.17}$	$3.36^{+0.17}_{-0.17}$	$3.36^{+0.17}_{-0.17}$	$3.36^{+0.16}_{-0.18}$	$3.36^{+0.17}_{-0.16}$
Planck15+SZ	$3.05^{+0.29}_{-0.29}$	$3.33^{+0.33}_{-0.34}$	$3.34^{+0.31}_{-0.31}$	$3.33^{+0.31}_{-0.31}$	$3.36^{+0.30}_{-0.30}$	$3.39^{+0.29}_{-0.29}$
Planck15+SZ+H_0	$3.30^{+0.19}_{-0.18}$	$3.39^{+0.19}_{-0.18}$	$3.39^{+0.18}_{-0.18}$	$3.38^{+0.19}_{-0.19}$	$3.38^{+0.19}_{-0.18}$	$3.39^{+0.19}_{-0.19}$

Table 4. 68% CI constraints on $N_{\rm eff}$ for various combinations of data and numbers of knots for the model cases where $N_{\rm eff}$ is allowed to vary in addition to the standard cosmological parameters and knots with k and amplitude freedom in position.

are provided by the latest intermediate results from Planck using low-ℓ HFI polarization [5], the data is not currently public. We use the interface provided by Cosmo++ to include the Planck 2015 likelihood code and use the full Planck CMB temperature power spectrum at multipoles $2 \leq \ell \leq 2500$ along with the Planck low-ℓ polarization likelihood in the range $2 \leq \ell \leq 29$. This combination of data is generally referred to as Planck TT+lowP. In this paper, we will refer to this combination of data as "Planck15."

Matter Power Spectrum.— In addition to CMB data, we also include power spectra measurements using two different data sets. The first data set comes from the SDSS Data Release 7 [55]. We use the most recent measure of the power spectrum of the reconstructed halo density field derived from a sample of 110,576 LRGs in Reid et al. [30]. As in the original analysis, we include modes up to an upper bound of $k_{\rm max} = 0.2\,h\,{\rm Mpc}^{-1}$, above which uncertainties in nonlinear corrections to the matter power spectrum become significant. The lower bound of $k_{\rm min} = 0.02\,h\,{\rm Mpc}^{-1}$ is a function of the survey volume. We have rewritten the original Reid et al. likelihood code in C++ in order to interface with Cosmo++. As in the original code, we include the effects on the linear power spectrum due to BAO damping, non-linear structure formation, and halo bias. We model each of these corrections identically to the original code, with the one difference being that we are using an updated version of Halofit [56, 57]. The fiducial model files have also been updated to include the effects of this new version of Halofit. We will use the shorthand "LRG" to refer to this set of data.

The second data set used for the matter power spectrum comes from the WiggleZ Dark Energy Survey, which provides a measurement of the matter power spectrum at redshifts $z = 0.22$, $z = 0.41$, $z = 0.60$, and $z = 0.78$ [31]. In our analysis, we include only modes that satisfy $0.02\,h\,{\rm Mpc}^{-1} < k < 0.2\,h\,{\rm Mpc}^{-1}$, as is done for the LRG data. Again, we have rewritten the WiggleZ likelihood code in C++ for use with Cosmo++ and compared the sampling results to those obtained with MontePython [58] to verify its accuracy. In this

paper, we will use "WZ" to refer to this data set.

Baryon Acoustic Oscillations.— We have included BAO data from the 6dFGS [32], from SDSS-MGS [33], and from BOSS Data Release 11, from both the LOWZ and CMASS samples [34]. We note that in cases where we use both LRG and BAO data, we omit the SDSS-MGS BAO data set in order to avoid double counting of information. For cases which do not include LRG, all four data sets are used when incorporating BAO measurements. From here on, we will refer to this data set simply as "BAO."

SZ Cluster Counts.— In addition, we include information from the detection of 189 clusters by *Planck* via the Sunyaev-Zeldovich effect [19]. Cosmological constraints were deduced in the $\sigma_8 - \Omega_m$ plane, which was found to be $\sigma_8(\Omega_M/0.27)^{0.3} = 0.764 \pm 0.025$ for the case where the hydrostatic bias $1 - b$ was allowed to vary in the range $[0.7, 1.0]$. The inclusion of this data will be referred to as "SZ."

Hubble Constant.— Finally, we include recent high-precision measures of the local Hubble expansion from the Hubble Space Telescope observations of Cepheid variables. This data was used to measure the local value of the Hubble Constant to 2.4%, as $H_0 = 73.02 \pm 1.79\,\mathrm{km\,s^{-1}\,Mpc^{-1}}$ [22]. This measurement will be referred to as "H_0." There are previous assessments of the local Hubble expansion that prefer lower values of H_0 [59]. We choose the Reiss et al. [22] determination because it addresses much of the issues raised in Efstathiou [59], and is the highest precision measurement of H_0 thus far. This result is also of interest since it indicates tension at low redshift, potentially from the same or different new physics leading to the tension in the cluster samples. We include the measure of H_0 to test what it indicates for ΛCDM in combination with Planck and cluster data.

3 Results and Discussion

Neutrino masses and $N_{\rm eff}$ with movable-knot PPS.— In Table 3, we report the 95% credible interval (CI) upper limits on the sum of the neutrino masses for zero to five knots for various combinations of data sets. The limits for the case with zero knots are consistent with previous work examining cosmological neutrino mass limits [60]. The last row of Table 3 shows the 68% CI constraints on $\sum m_\nu$ when SZ is included along with Planck15. This shows a preference for non-zero $\sum m_\nu$, indicating some tension with the other data sets in this analysis. For each of these cases, $\sum m_\nu$ is allowed to vary in addition to the other standard cosmological parameters, along with the knot locations and amplitudes. When the knot location is allowed to vary freely, the constraints on $\sum m_\nu$ show no dependence on the number of knots in our Monte Carlo analysis. Therefore, for reconstructions of this form, constraints on $\sum m_\nu$ appear to be robust to changes in the shape of the PPS.

Furthermore, our most stringent limit achieved using the combination of data sets Planck15+LRG+BAO+H_0 of $\sum m_\nu \lesssim 0.13\,\mathrm{eV}$ with one interior knot is comparable to the constraint obtained with the ΛCDM spectrum (matching the same analysis in Ref. [61]). This is beginning to approach the minimum allowed value for the inverted neutrino mass hierarchy of $\sum m_\nu \sim 0.1\,\mathrm{eV}$ and suggests that future precision measurements could distinguish between the two possibilities for the neutrino mass hierarchy. Joint constraints on σ_8, h, $N_{\rm eff}$, and $\sum m_\nu$ shown in Fig. 1, illustrate how neutrino constraints become tighter with the inclusion of additional data sets and which data most significantly impact the constraints. We find that inclusion of the BAO data provides the most significant improvement in the

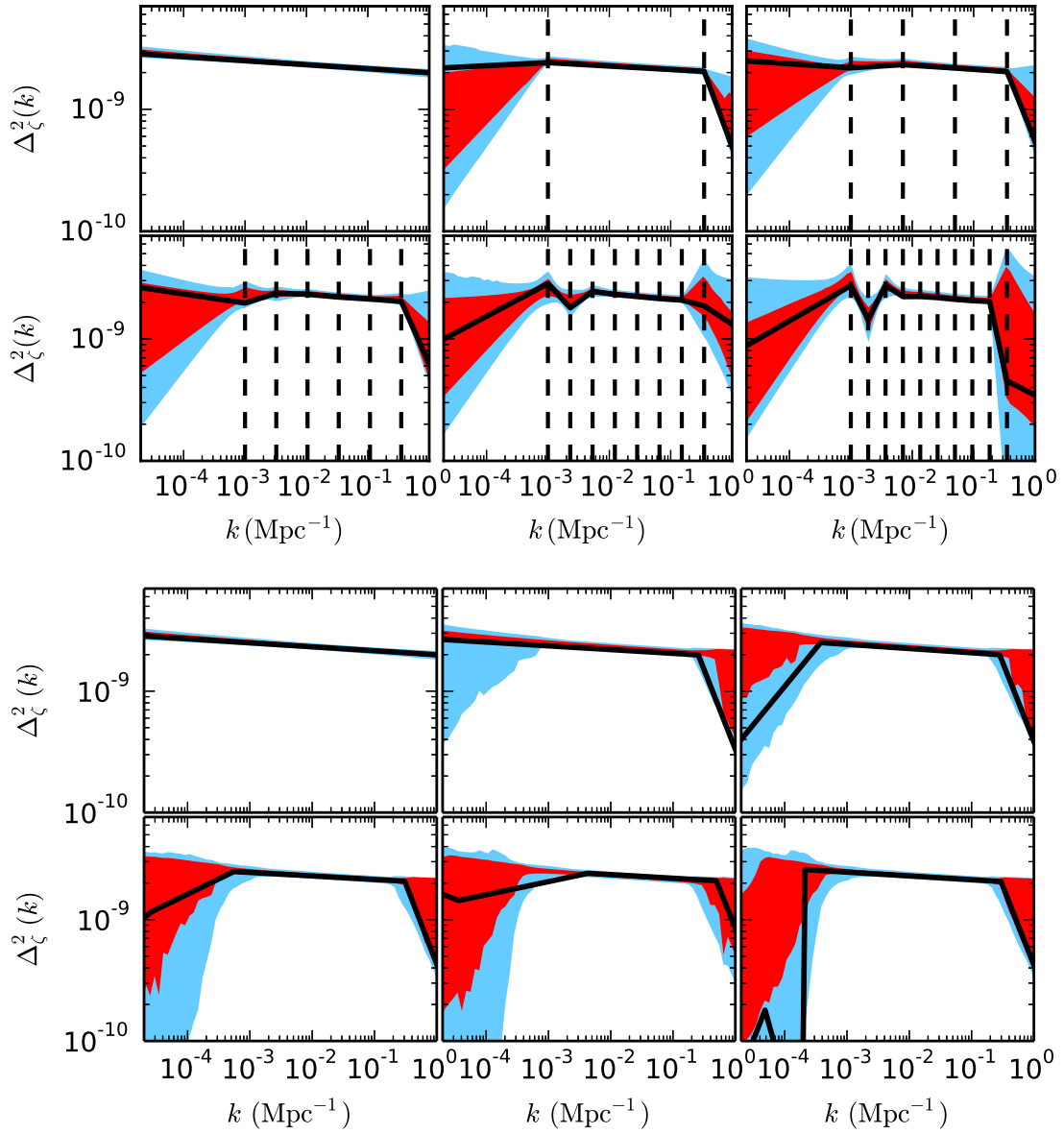

Figure 6. Shown *(top)* are the PPS estimated using Planck15 data for the case where the knot locations are fixed and only the amplitudes are varied, along with $\sum m_\nu$ to vary. The black line shows the best fit PPS, and the red and blue regions correspond to the 68% and 95% CI regions. We see similar reconstructed power spectra when BAO is included *(not shown)*. For comparison, we show *(bottom)* the same PPS with between 0 to 5 knots, so the corresponding panels in the top and bottom figure have the same number of free parameters.

limit on the sum of neutrino masses due to the complementarity of BAO in constraining Ω_m, which is highly degenerate with $\sum m_\nu$. The change in the posterior distributions for varying numbers of knots and combinations of data sets are shown in Fig. 2, demonstrating again the fact that allowing for additional freedom in the PPS does not significantly impact neutrino parameter constraints. Knots beyond two are not shown as they do not change the posterior distribution in a noticeable manner.

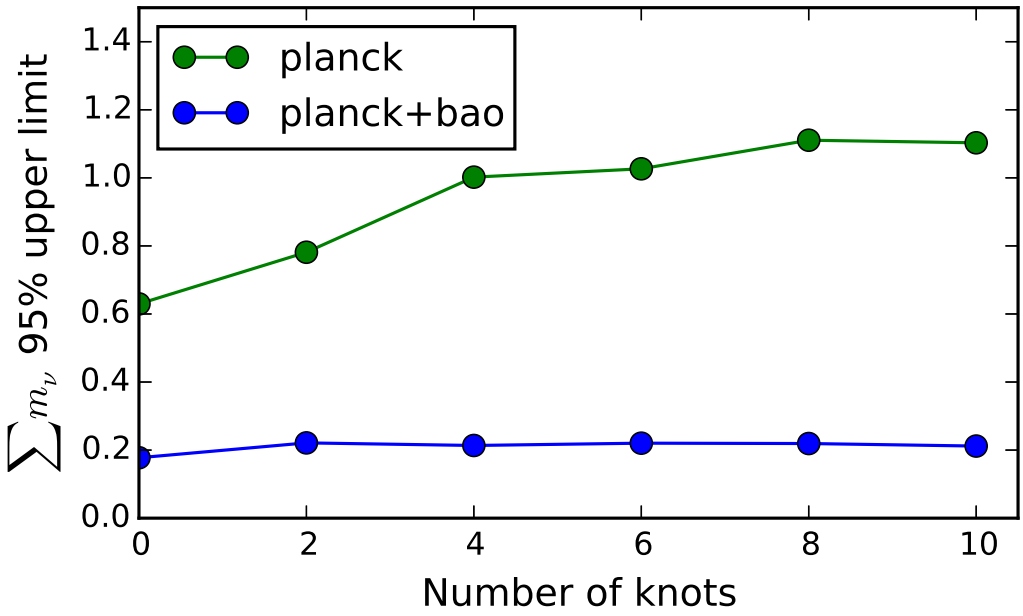

Figure 7. Shown are the 95% CI upper limits on $\sum m_\nu$ for fixed knot locations when only Planck15 data is included and when Planck15+BAO are included.

Table 4 shows the derived constraints on $N_{\rm eff}$ for zero to five knots for various combinations of data sets. In these cases, $N_{\rm eff}$ is allowed to vary along with the other standard cosmological parameters, along with the PPS knot locations and amplitudes. As with $\sum m_\nu$, constraints on $N_{\rm eff}$ also appear to be robust to a relaxation of the assumption that the PPS adheres to a power-law shape. In all cases in which H_0 is included, the best fit value for $N_{\rm eff}$ is observed to shift up, such that the standard value of 3.046 lies just outside the 95% allowed region for the majority of cases. Limits on $N_{\rm eff}$ are shown in Fig. 3. The dependence of the one-dimensional posterior distributions for $\sum m_\nu$ and $N_{\rm eff}$ are shown in Fig. 4. As mentioned, very little change is present when going from 0 to 2 knots. Beyond 2 knots, there is no discernible change, and so only cases up to 2 knots are shown.

Comparing fixed and movable-knot PPS.— To test how differences in methods for reconstructing the PPS affect derived neutrino parameter constraints, we perform several runs in which we fix the position of the knots in a similar manner to the method used in Ref. [27]. Fig. 5 shows how the posterior distribution of $\sum m_\nu$ changes in the case where the position of knots are fixed and only the amplitudes are allowed to vary. For these cases, we follow a similar procedure to that described above for our "knot-spline" reconstruction, with the exception that the position of the knots are fixed in k-space. We perform runs with 0, 2, 4, 6, 8, and 10 knots, with locations indicated by the vertical dotted lines in Fig. 6.

For the case where only Planck15 is included, the posterior distribution of $\sum m_\nu$ varies considerably. This contrasts with our reconstruction in which the knot location is allowed to vary, indicating that the neutrino parameter constraints are sensitive to the prior on the allowed shape of the PPS. However, when information from LSS is included, in this case in the form of BAO data, the degree of change is significantly less. This is not surprising given

the fact that LSS is expected to be a much more sensitive probe of neutrino mass than CMB measurements alone. The 95% upper limits on $\sum m_\nu$ are shown in Fig. 7, illustrating this difference. The PPS for our fixed-location knots are shown in Fig. 6. These figures indicate more of a preference for features in the PPS relative to the reconstruction method in which the knot locations are allowed to vary freely.

In Fig. 9, we show the reconstructed PPS for cosmological models with different number of knots for Planck15 combined with various combinations of LRG, BAO, SZ, and H_0 data sets. We find no significant features in the PPS using Planck15 with any combination of LRG, WZ, and BAO data. There is some apparent evidence for features when using the tension data sets SZ and H_0 which will be discussed in more detail later in this paper. The black lines represent the most likely power spectra. These all tend to recover the standard power-law form for the PPS at small scales $k \gtrsim 10^{-3}\,\mathrm{Mpc}^{-1}$. At larger scales $k \lesssim 10^{-3}\,\mathrm{Mpc}^{-1}$, the best fit power spectra for models with non-zero numbers of knots tend to indicate a suppression of power at large scales due to the well-known low C_ℓ at low ℓ in the CMB (see, *e.g.* Ref. [28]). Note that when allowing the knot positions to freely vary, they accumulate in the cosmic variance dominated region, so that functions with a fixed amount of variability will prefer to fit large scale features preferably than small scale ones. Since we do not have *a priori* knowledge of the position of features in the PPS, we allow the knot location to vary. Furthermore, relaxing the position of the features protects against the look-elsewhere effect or multiple comparisons problem, since the knot is free to move over the global range of k.

The confidence ranges for the power spectra in Figs. 6, 8 and 9 are calculated as follows. For each k value we construct a sample of all $P(k)$ values from our sample of power spectra, and from that sample we calculate the confidence intervals. The confidence intervals are constructed around the median of the sample, so that e.g. the 68% confidence interval leaves out 16% of the points of the sample on each side. This is the reason why the best fit lines sometimes lie outside the 68% confidence range.

Table 5 shows the $\Delta \ln(Z)$ values for the free and fixed-knot location PPS reconstructions described above with $\sum m_\nu$ free. In most cases, particularly for DOF ≥ 4, Bayesian evidence strongly prefers the reconstruction in which the knot location is free over models with knots fixed at the positions shown in Fig. 6. This indicates that a simple power-law fit over the approximate range $10^{-3}\,\mathrm{Mpc}^{-1} < k < 1\,\mathrm{Mpc}^{-1}$ provides a significantly better fit than the hint of features seen in the PPS for fixed knot positions.

We should note that the big change in Bayesian evidences for the fixed knots case depends on the prior. The change would not be so dramatic if we had chosen a smaller prior range for $\log(10^{10}\Delta^2_{\rm knot})$. Although we use the same prior for the moveable knots case, we do not see such large changes in the evidence because the knots are able to move to parts of the parameter region where there is high cosmic variance or noise, unless there are actual features to fit. For the fixed knots case, however, there is only freedom to fit features at a priori fixed locations, and if there are none then we see a significant drop in evidence.

Model comparison.— The change in Bayesian evidence relative to the six-parameter ΛCDM model is shown in Table 6 for the data sets Planck15+LRG+BAO(+H_0). Importantly, there is no significant preference for any model that includes $\sum m_\nu$, $N_{\rm eff}$, or knots over a simple ΛCDM model. The six-parameter ΛCDM model is also preferred with Planck15 data alone.

However, with the inclusion of the recent measurement of H_0, there is a significant preference for the combination of additional parameters $N_{\rm eff}$ and knots. The cases with 2, 4, and

Planck15			Planck15+BAO		
DOF	$\Delta \ln(Z)$ Free	$\Delta \ln(Z)$ Fixed	DOF	$\Delta \ln(Z)$ Free	$\Delta \ln(Z)$ Fixed
2	1.26	1.15	2	1.25	1.24
4	1.15	−5.79	4	1.2	−6.52
6	1.48	−13.03	6	1.42	−13.5
8	0.81	−20.33	8	1.07	−18.74
10	0.47	−21.59	10	1.21	−22.47

Table 5. Comparison of $\Delta \ln(Z)$ values relative to the 0 knot case (ΛCDM) for free-form PPS models with knot position in $\log_{10} k$ either free or fixed. For all cases, $\sum m_\nu$ is also free. The number of knots for each case is such that the number of additional degrees of freedom is equal in each row. For example, two additional degrees of freedom in the PPS corresponds to one knot in the free case (location and amplitude) and two knots in the fixed case (amplitude of each knot).

Planck15+LRG+BAO		Planck15+LRG+BAO+H_0	
Model	$\Delta \ln(Z)$	Model	$\Delta \ln(Z)$
ΛCDM	—	ΛCDM	—
+1 knot	0.99	+1 knot	1.60
+2 knots	1.07	+2 knots	1.15
+3 knots	0.75	+3 knots	1.40
+4 knots	0.61	+4 knots	1.31
+5 knots	0.59	+5 knots	0.78
—	—	$+N_{\rm eff}$+1 knot	1.13
$+N_{\rm eff}$+2 knots	0.10	$+N_{\rm eff}$+2 knots	1.43
—	—	$+N_{\rm eff}$+3 knots	0.74
—	—	$+N_{\rm eff}$+4 knots	1.25
—	—	$+N_{\rm eff}$+5 knots	0.89

Table 6. $\Delta \ln(Z)$ values relative to the six parameter ΛCDM model for various cosmological models for the combination of data sets Planck15+LRG+BAO and when H_0 is added. Only models for which $\Delta \ln(Z)$ is positive relative to ΛCDM are shown.

5 knots all satisfy $\Delta \ln(Z) > 2.5$, which can be interpreted as "strong" or "significant" odds against ΛCDM. The Bayes factor for all models with positive $\Delta \ln(Z)$ for the Planck15+H_0 likelihood are shown in Table 7.

Similarly, when the SZ data set is included with Planck15, there is a significant preference for the combination of a nonzero number of knots along with a nonzero value for the

sum of the neutrino masses (see Table 3 for Planck15+SZ). When H_0 is also included, we see evidence for knots and $N_{\rm eff}$. This comes largely from $N_{\rm eff}$ enhancing the diffusion damping of the CMB anisotropies, which is recovered by a larger H_0 in order to preserve the position of the acoustic peaks (see, e.g. [**?**]). Table 8 shows the Bayes factor for both of these cases, Planck15+SZ and Planck15+SZ+H_0. There is a significant preference for cosmological models with zero to five knots, with $\Delta \ln(Z) > 2.5$ for several model cases that contain additional non-standard cosmological parameters. For the combination of data sets Planck15+SZ+H_0, a cosmological model with 3 knots is heavily favored with $\Delta \ln(Z) > 5$. If we can assume that the tension data set SZ is an accurate measurement, as well as the measurement of H_0, then these results represent strong evidence that the PPS contains non-trivial features, not captured by a power-law representation. In particular, for this case, we see a preference for a very sharp cutoff at high k, as shown in Fig. 8. The cutoff in power at high k provides the smaller amplitude in power indicated by the SZ measurements. More conservatively, this is an indication that there are systematic effects within the data that mimic PPS features, which warrant further investigation. Importantly, smaller scale measures of the PPS such as the Lyman-α forest would add more information and likely disfavor strong departures from a power-law PPS (e.g. [62]), but including the inferred matter power spectrum from the Lyman-α forest is beyond the scope of the current work.

4 Conclusion

Using data from a broad set of the most recent cosmological observations, including CMB, BAO, power spectrum, cluster counts, and Hubble constant measurements, we have examined the dependence on the assumed form of the PPS in measures of neutrino parameters $\sum m_\nu$ and $N_{\rm eff}$. To do this, we applied the "knot-spline" method for reconstructing the PPS, following [28, 29, 41], and allowing the knot positions to vary in location as well as amplitude.

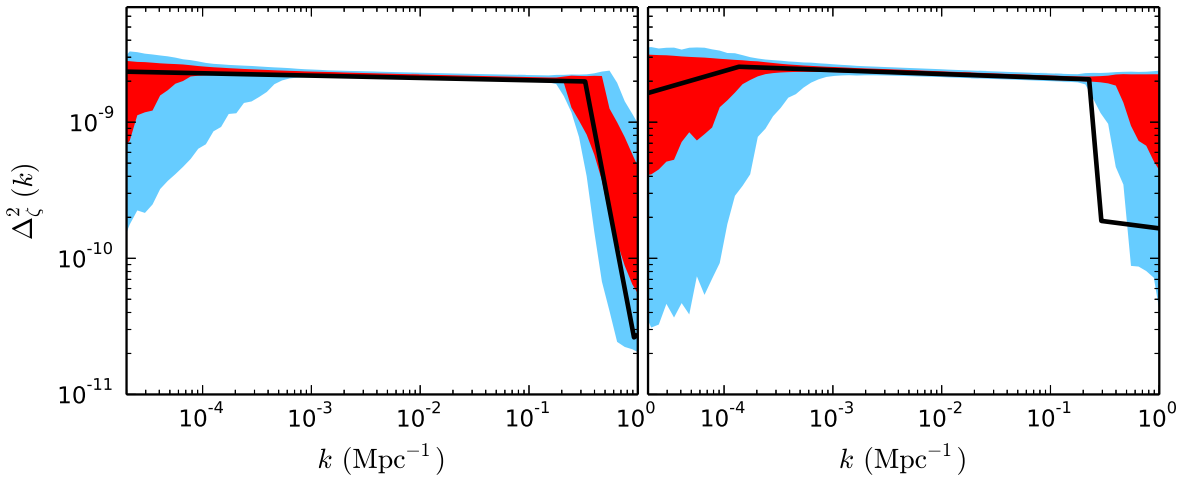

Figure 8. Shown *(left)* is the PPS for Planck15+SZ+H_0 with 3 knots, which corresponds to our model with the highest evidence. For comparison, we also show *(right)* the three knot case with only Planck15 data included. The black solid lines show the best-fit PPS, the red lines are PPS in the 68% CI, and the light blue lines are the PPS that fall in the 95% CI (note that it is possible for the PPS belonging to the sample with the maximum likelihood value to lie outside the red or blue regions).

Planck15		Planck15+H_0	
Model	$\Delta \ln(Z)$	Model	$\Delta \ln(Z)$
ΛCDM	—	ΛCDM	—
—	—	$+N_{\rm eff}$	0.49
+1 knot	1.00	+1 knot	1.56
+2 knots	1.18	+2 knots	2.02
+3 knots	1.68	+3 knots	1.72
+4 knots	0.91	+4 knots	2.05
+5 knots	0.60	+5 knots	1.92
$+N_{\rm eff}$+1 knot	0.40	$+N_{\rm eff}$+1 knot	2.27
$+N_{\rm eff}$+2 knots	0.45	$+N_{\rm eff}$+2 knots	*2.64*
$+N_{\rm eff}$+3 knots	0.13	$+N_{\rm eff}$+3 knots	2.43
$+N_{\rm eff}$+4 knots	0.50	$+N_{\rm eff}$+4 knots	*3.08*
—	—	$+N_{\rm eff}$+5 knots	*2.69*

Table 7. $\Delta \ln(Z)$ values relative to ΛCDM for various cosmological models for Planck15 and when H_0 is added. Only models for which $\Delta \ln(Z)$ is positive relative to ΛCDM are shown.

We found that for this method of reconstruction, measures of $N_{\rm eff}$ and $\sum m_\nu$ do not appear to depend strongly on assumptions about the PPS. However, when the knot location is fixed, with CMB data alone, we observe a strong dependency between $\sum m_\nu$ and the prior on the PPS. While including information from LSS mitigates much of this dependency, this work underscores the importance of quantifying the dependence of parameter constraints on model assumptions and demonstrates the sensitivity of neutrino parameter constraints on PPS priors and choice of data sets.

For combinations of data which include Planck15, BAO, LRG, and WZ, we see no evidence for features in the PPS or a non-zero number of knots. In addition, there is no preference for significant non-zero neutrino mass or a value for $N_{\rm eff}$ outside of the standard value expected in ΛCDM. Significantly, when we include recent high-precision measurements of the low-redshift Hubble constant, we find no significant evidence for extra relativistic energy density $N_{\rm eff}$. However, we do see relatively significant evidence for a non-zero number of knots in concert with a value for $N_{\rm eff}$ that diverges from the standard value. When including the tension data from SZ cluster counts, we see weak evidence for non-zero neutrino mass and more significant evidence for knots or knots with $N_{\rm eff}$ and $\sum m_\nu$. However, when both H_0 and SZ measurements are included, the preference for $\sum m_\nu$ vanishes, and only models which allow for both $N_{\rm eff}$ and knots to vary are favored, with a model containing only 3 knots in addition to the standard ΛCDM cosmological parameters being preferred the most strongly over ΛCDM. The radical difference in the Bayesian evidences obtained for extensions to the 6-parameter ΛCDM model with combinations of these data most conservatively points to some unmodeled systematic effect, rather than a coherent body of evidence in favor of

Planck15+SZ		Planck15+SZ+H_0	
Model	$\Delta \ln(Z)$	Model	$\Delta \ln(Z)$
ΛCDM	—	ΛCDM	—
$+\sum m_\nu$	1.41	—	—
+1 knot	*2.65*	+1 knot	*3.09*
+2 knots	*2.78*	+2 knots	*3.48*
+3 knots	*3.06*	+3 knots	**5.03**
+4 knots	*4.37*	+4 knots	*4.74*
+5 knots	*4.33*	+5 knots	*2.94*
$+\sum m_\nu$+1 knot	*3.75*	—	—
$+\sum m_\nu$+2 knots	*3.49*	—	—
$+\sum m_\nu$+3 knots	*3.33*	$+\sum m_\nu$+3 knots	1.60
$+\sum m_\nu$+4 knots	*4.39*	—	—
$+\sum m_\nu$+5 knots	*4.49*	$+\sum m_\nu$+5 knots	1.50
$+N_{\rm eff}$+1 knot	2.05	$+N_{\rm eff}$+1 knot	*3.46*
$+N_{\rm eff}$+2 knots	2.28	$+N_{\rm eff}$+2 knots	*3.36*
$+N_{\rm eff}$+3 knots	2.00	$+N_{\rm eff}$+3 knots	*3.09*
$+N_{\rm eff}$+4 knots	1.76	$+N_{\rm eff}$+4 knots	*3.21*
$+N_{\rm eff}$+5 knots	*3.69*	$+N_{\rm eff}$+5 knots	*3.25*
$+N_{\rm eff}+\sum m_\nu$+1 knot	2.49	$+N_{\rm eff}+\sum m_\nu$+1 knot	1.77
$+N_{\rm eff}+\sum m_\nu$+2 knots	*2.60*	$+N_{\rm eff}+\sum m_\nu$+2 knots	2.17
$+N_{\rm eff}+\sum m_\nu$+3 knots	2.46	$+N_{\rm eff}+\sum m_\nu$+3 knots	*3.59*
$+N_{\rm eff}+\sum m_\nu$+4 knots	*2.81*	$+N_{\rm eff}+\sum m_\nu$+4 knots	*3.41*
$+N_{\rm eff}+\sum m_\nu$+5 knots	*3.71*	$+N_{\rm eff}+\sum m_\nu$+5 knots	*3.39*

Table 8. $\Delta \ln(Z)$ values relative to 6-parameter ΛCDM for various cosmological models for the combination of data sets Planck15+SZ and when H_0 is added. Only models for which $\Delta \ln(Z) > 1.0$ relative to ΛCDM are shown. Significantly, there is no preference for neither extra relativistic degrees of freedom in $N_{\rm eff}$ nor non-zero $\sum m_\nu$.

non-standard cosmology. The tension data could also indicate non-standard background expansion histories [**?**].

As a combination of low, medium and high-redshift probes are complementarily combined to constrain expansion history, cosmological matter, dark energy, neutrino densities, and the primordial power spectrum, robust methods of indications of new model features

and measures of new physics should be employed. Our work finds that relaxing *a priori* assumptions of the scales of features in the primordial power spectrum does not significantly alleviate constraints on neutrino mass and relativistic energy density. Significantly, we find the tension in cosmological data from representative cluster data sets do not significantly indicate a non-zero measure of massive neutrinos. Also, we find the tension from Planck 2015 CMB and recent high-precision H_0 measures give no preference for a non-standard $N_{\rm eff}$. As cosmology enters an increasingly high-precision era with multiple epoch and physical scale probes, robust statistical methods and model tests will continue to be needed in order to make claims for the discovery of new physics.

Acknowledgments

We thank Asantha Cooray, Elena Giusarma, and Manoj Kaplinghat for useful discussions. We acknowledge the use of the New Zealand eScience Infrastructure (NeSI) high-performance computing facilities, which are funded jointly by NeSI's collaborator institutions and through the Ministry of Business, Innovation & Employment's Research Infrastructure programme [http://www.nesi.org.nz]. NC and KNA are partially supported by NSF CAREER Grant No. PHY-1159224 and NSF Grant No. PHY-1316792. LCP is supported by the DOE DE-SC0011114 grant. KNA acknowledges hospitality and support by the Mainz Institute for Theoretical Physics (MITP) program on "Exploring the Energy Ladder of the Universe" where a portion of this work was completed.

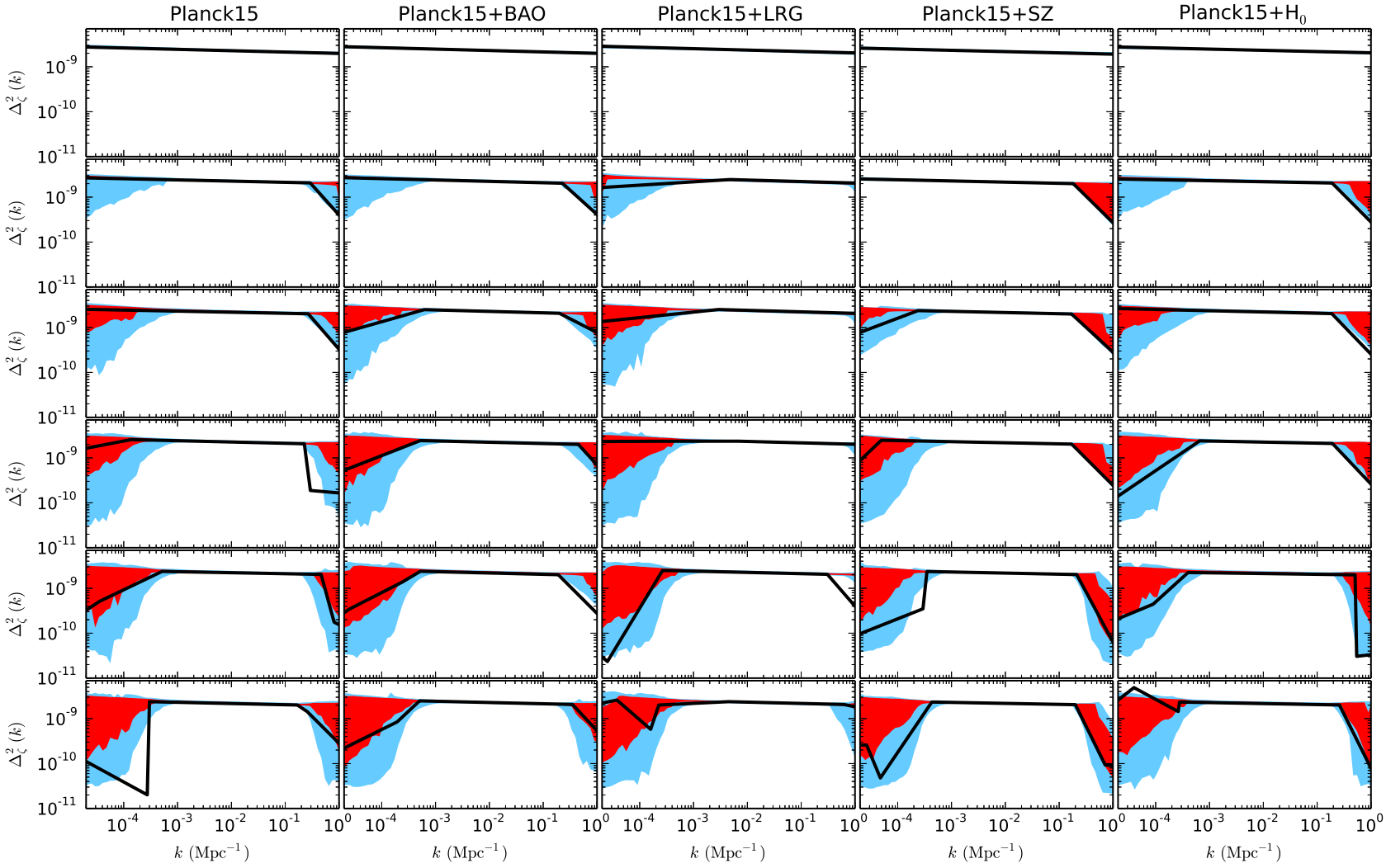

Figure 9. The reconstructed primordial power spectrum (PPS) without varying neutrino parameters. The columns correspond to different data sets used, shown at the top of each column. The number of knots increases from 0 to 5 from top to bottom. The black solid lines show the best-fit PPS, the red lines are PPS in the 68% CI, and the light blue lines are the PPS that fall in the 95% CI.

References

[1] W. Hu, D. J. Eisenstein, and M. Tegmark, *Weighing neutrinos with galaxy surveys*, *Phys. Rev. Lett.* **80** (1998) 5255–5258, [astro-ph/9712057].

[2] K. N. Abazajian and M. Kaplinghat, *Neutrino Physics from the Cosmic Microwave Background and Large Scale Structure*, *Ann. Rev. Nucl. and Part. Phys.* (2016). in press.

[3] **Planck** Collaboration, P. A. R. Ade et al., *Planck 2015 results. XIII. Cosmological parameters*, arXiv:1502.01589.

[4] **Particle Data Group** Collaboration, K. A. Olive et al., *Review of Particle Physics*, *Chin. Phys.* **C38** (2014) 090001.

[5] **Planck** Collaboration, N. Aghanim et al., *Planck 2016 intermediate results. XLVI. Reduction of large-scale systematic effects in HFI polarization maps and estimation of the reionization optical depth*, arXiv:1605.02985.

[6] Z. Hou et al., *Constraints on Cosmology from the Cosmic Microwave Background Power Spectrum of the 2500 deg^2 SPT-SZ Survey*, *Astrophys. J.* **782** (2014) 74, [arXiv:1212.6267].

[7] R. A. Battye and A. Moss, *Evidence for Massive Neutrinos from Cosmic Microwave Background and Lensing Observations*, *Phys. Rev. Lett.* **112** (2014), no. 5 051303, [arXiv:1308.5870].

[8] **BOSS** Collaboration, F. Beutler et al., *The clustering of galaxies in the SDSS-III Baryon Oscillation Spectroscopic Survey: Signs of neutrino mass in current cosmological datasets*, *Mon. Not. Roy. Astron. Soc.* **444** (2014) 3501, [arXiv:1403.4599].

[9] M. Wyman, D. H. Rudd, R. A. Vanderveld, and W. Hu, *Neutrinos Help Reconcile Planck Measurements with the Local Universe*, *Phys. Rev. Lett.* **112** (2014), no. 5 051302, [arXiv:1307.7715].

[10] L. Verde, P. Protopapas, and R. Jimenez, *Planck and the local Universe: Quantifying the tension*, *Phys. Dark Univ.* **2** (2013) 166–175, [arXiv:1306.6766].

[11] R. A. Battye, T. Charnock, and A. Moss, *Tension between the power spectrum of density perturbations measured on large and small scales*, *Phys. Rev.* **D91** (2015), no. 10 103508, [arXiv:1409.2769].

[12] E. Giusarma, E. Di Valentino, M. Lattanzi, A. Melchiorri, and O. Mena, *Relic Neutrinos, thermal axions and cosmology in early 2014*, *Phys. Rev.* **D90** (2014), no. 4 043507, [arXiv:1403.4852].

[13] M. Roncarelli, C. Carbone, and L. Moscardini, *The effect of massive neutrinos on the SunyaevZel'dovich and X-ray observables of galaxy clusters*, *Mon. Not. Roy. Astron. Soc.* **447** (2015), no. 2 1761–1773, [arXiv:1409.4285].

[14] M. Raveri, *Are cosmological data sets consistent with each other within the Λ cold dark matter model?*, *Phys. Rev.* **D93** (2016), no. 4 043522, [arXiv:1510.00688].

[15] L. Verde, S. M. Feeney, D. J. Mortlock, and H. V. Peiris, *(Lack of) Cosmological evidence for dark radiation after Planck*, *JCAP* **1309** (2013) 013, [arXiv:1307.2904].

[16] B. Leistedt, H. V. Peiris, and L. Verde, *No new cosmological concordance with massive sterile neutrinos*, *Phys. Rev. Lett.* **113** (2014) 041301, [arXiv:1404.5950].

[17] N. MacCrann, J. Zuntz, S. Bridle, B. Jain, and M. R. Becker, *Cosmic Discordance: Are Planck CMB and CFHTLenS weak lensing measurements out of tune?*, *Mon. Not. Roy. Astron. Soc.* **451** (2015), no. 3 2877–2888, [arXiv:1408.4742].

[18] **SPT** Collaboration, A. Saro et al., *Constraints on the CMB temperature evolution using multiband measurements of the SunyaevZel'dovich effect with the South Pole Telescope*, *Mon.*

Not. Roy. Astron. Soc. **440** (2014), no. 3 2610–2615, [arXiv:1312.2462].

[19] **Planck** Collaboration, P. A. R. Ade et al., *Planck 2013 results. XX. Cosmology from SunyaevZeldovich cluster counts*, *Astron. Astrophys.* **571** (2014) A20, [arXiv:1303.5080].

[20] A. Vikhlinin et al., *Chandra Cluster Cosmology Project III: Cosmological Parameter Constraints*, *Astrophys. J.* **692** (2009) 1060–1074, [arXiv:0812.2720].

[21] **DSDD** Collaboration, E. Rozo et al., *Cosmological Constraints from the SDSS maxBCG Cluster Catalog*, *Astrophys. J.* **708** (2010) 645–660, [arXiv:0902.3702].

[22] A. G. Riess et al., *A 2.4% Determination of the Local Value of the Hubble Constant*, arXiv:1604.01424.

[23] K. N. Abazajian et al., *Cosmological and Astrophysical Neutrino Mass Measurements*, *Astropart. Phys.* **35** (2011) 177–184, [arXiv:1103.5083].

[24] W. H. Kinney, *How to fool cosmic microwave background parameter estimation*, *Phys. Rev.* **D63** (2001) 043001, [astro-ph/0005410].

[25] R. de Putter, E. V. Linder, and A. Mishra, *Inflationary Freedom and Cosmological Neutrino Constraints*, *Phys. Rev.* **D89** (2014), no. 10 103502, [arXiv:1401.7022].

[26] S. Gariazzo, C. Giunti, and M. Laveder, *Light Sterile Neutrinos and Inflationary Freedom*, *JCAP* **1504** (2015), no. 04 023, [arXiv:1412.7405].

[27] E. Di Valentino, S. Gariazzo, M. Gerbino, E. Giusarma, and O. Mena, *Dark Radiation and Inflationary Freedom after Planck 2015*, *Phys. Rev.* **D93** (2016), no. 8 083523, [arXiv:1601.07557].

[28] G. Aslanyan, L. C. Price, K. N. Abazajian, and R. Easther, *The Knotted Sky I: Planck constraints on the primordial power spectrum*, *JCAP* **1408** (2014) 052, [arXiv:1403.5849].

[29] K. N. Abazajian, G. Aslanyan, R. Easther, and L. C. Price, *The Knotted Sky II: Does BICEP2 require a nontrivial primordial power spectrum?*, *JCAP* **1408** (2014) 053, [arXiv:1403.5922].

[30] B. A. Reid et al., *Cosmological Constraints from the Clustering of the Sloan Digital Sky Survey DR7 Luminous Red Galaxies*, *Mon. Not. Roy. Astron. Soc.* **404** (2010) 60–85, [arXiv:0907.1659].

[31] D. Parkinson et al., *The WiggleZ Dark Energy Survey: Final data release and cosmological results*, *Phys. Rev.* **D86** (2012) 103518, [arXiv:1210.2130].

[32] F. Beutler, C. Blake, M. Colless, D. H. Jones, L. Staveley-Smith, L. Campbell, Q. Parker, W. Saunders, and F. Watson, *The 6dF Galaxy Survey: Baryon Acoustic Oscillations and the Local Hubble Constant*, *Mon. Not. Roy. Astron. Soc.* **416** (2011) 3017–3032, [arXiv:1106.3366].

[33] A. J. Ross, L. Samushia, C. Howlett, W. J. Percival, A. Burden, and M. Manera, *The clustering of the SDSS DR7 main Galaxy sample I. A 4 per cent distance measure at* $z = 0.15$, *Mon. Not. Roy. Astron. Soc.* **449** (2015), no. 1 835–847, [arXiv:1409.3242].

[34] **BOSS** Collaboration, L. Anderson et al., *The clustering of galaxies in the SDSS-III Baryon Oscillation Spectroscopic Survey: baryon acoustic oscillations in the Data Releases 10 and 11 Galaxy samples*, *Mon. Not. Roy. Astron. Soc.* **441** (2014), no. 1 24–62, [arXiv:1312.4877].

[35] G. Aslanyan, *Cosmo++: An Object-Oriented C++ Library for Cosmology*, *Comput. Phys. Commun.* **185** (2014) 3215–3227, [arXiv:1312.4961].

[36] J. Lesgourgues, *The Cosmic Linear Anisotropy Solving System (CLASS) I: Overview*, arXiv:1104.2932.

[37] D. Blas, J. Lesgourgues, and T. Tram, *The Cosmic Linear Anisotropy Solving System (CLASS) II: Approximation schemes*, *JCAP* **1107** (2011) 034, [arXiv:1104.2933].

[38] F. Feroz and M. P. Hobson, *Multimodal nested sampling: an efficient and robust alternative to MCMC methods for astronomical data analysis*, *Mon. Not. Roy. Astron. Soc.* **384** (2008) 449, [arXiv:0704.3704].

[39] F. Feroz, M. P. Hobson, and M. Bridges, *MultiNest: an efficient and robust Bayesian inference tool for cosmology and particle physics*, *Mon. Not. Roy. Astron. Soc.* **398** (2009) 1601–1614, [arXiv:0809.3437].

[40] F. Feroz, M. P. Hobson, E. Cameron, and A. N. Pettitt, *Importance Nested Sampling and the MultiNest Algorithm*, arXiv:1306.2144.

[41] J. A. Vazquez, M. Bridges, M. P. Hobson, and A. N. Lasenby, *Model selection applied to reconstruction of the Primordial Power Spectrum*, *JCAP* **1206** (2012) 006, [arXiv:1203.1252].

[42] C. Sealfon, L. Verde, and R. Jimenez, *Smoothing spline primordial power spectrum reconstruction*, *Phys. Rev.* **D72** (2005) 103520, [astro-ph/0506707].

[43] M. Bridges, A. N. Lasenby, and M. P. Hobson, *A bayesian analysis of the primordial power spectrum*, *Mon. Not. Roy. Astron. Soc.* **369** (2006) 1123–1130, [astro-ph/0511573].

[44] M. Bridges, A. N. Lasenby, and M. P. Hobson, *WMAP 3-year primordial power spectrum*, *Mon. Not. Roy. Astron. Soc.* **381** (2007) 68–74, [astro-ph/0607404].

[45] L. Verde and H. V. Peiris, *On Minimally-Parametric Primordial Power Spectrum Reconstruction and the Evidence for a Red Tilt*, *JCAP* **0807** (2008) 009, [arXiv:0802.1219].

[46] M. Bridges, F. Feroz, M. P. Hobson, and A. N. Lasenby, *Bayesian optimal reconstruction of the primordial power spectrum*, *Mon. Not. Roy. Astron. Soc.* **400** (2009) 1075–1084, [arXiv:0812.3541].

[47] H. V. Peiris and L. Verde, *The Shape of the Primordial Power Spectrum: A Last Stand Before Planck*, *Phys. Rev.* **D81** (2010) 021302, [arXiv:0912.0268].

[48] S. Bird, H. V. Peiris, M. Viel, and L. Verde, *Minimally Parametric Power Spectrum Reconstruction from the Lyman-alpha Forest*, *Mon. Not. Roy. Astron. Soc.* **413** (2011) 1717–1728, [arXiv:1010.1519].

[49] J. A. Vazquez, A. N. Lasenby, M. Bridges, and M. P. Hobson, *A Bayesian study of the primordial power spectrum from a novel closed universe model*, *Mon. Not. Roy. Astron. Soc.* **422** (2012) 1948–1956, [arXiv:1103.4619].

[50] **Planck** Collaboration, P. A. R. Ade et al., *Planck 2015 results. XX. Constraints on inflation*, arXiv:1502.02114.

[51] A. Ravenni, L. Verde, and A. J. Cuesta, *Red, Straight, no bends: primordial power spectrum reconstruction from CMB and large-scale structure*, arXiv:1605.06637.

[52] H. Jeffreys, *Theory of Probability*. Oxford University Press, 1961.

[53] M. P. Hobson, A. H. Jaffe, A. R. Liddle, P. Mukherjee, and D. Parkinson, *Bayesian methods in cosmology*. Cambridge University Press, 2010.

[54] **Planck** Collaboration, R. Adam et al., *Planck 2015 results. I. Overview of products and scientific results*, arXiv:1502.01582.

[55] **SDSS** Collaboration, K. N. Abazajian et al., *The Seventh Data Release of the Sloan Digital Sky Survey*, *Astrophys. J. Suppl.* **182** (2009) 543–558, [arXiv:0812.0649].

[56] R. Takahashi, M. Sato, T. Nishimichi, A. Taruya, and M. Oguri, *Revising the Halofit Model for the Nonlinear Matter Power Spectrum*, *Astrophys. J.* **761** (2012) 152, [arXiv:1208.2701].

[57] S. Bird, M. Viel, and M. G. Haehnelt, *Massive Neutrinos and the Non-linear Matter Power Spectrum*, *Mon. Not. Roy. Astron. Soc.* **420** (2012) 2551–2561, [arXiv:1109.4416].

[58] B. Audren, J. Lesgourgues, K. Benabed, and S. Prunet, *Conservative Constraints on Early*

Cosmology: an illustration of the Monte Python cosmological parameter inference code, *JCAP* **1302** (2013) 001, [arXiv:1210.7183].

[59] G. Efstathiou, *H0 Revisited*, *Mon. Not. Roy. Astron. Soc.* **440** (2014), no. 2 1138–1152, [arXiv:1311.3461].

[60] A. J. Cuesta, V. Niro, and L. Verde, *Neutrino mass limits: robust information from the power spectrum of galaxy surveys*, arXiv:1511.05983.

[61] E. Giusarma, M. Gerbino, O. Mena, S. Vagnozzi, S. Ho, and K. Freese, *On the improvement of cosmological neutrino mass bounds*, arXiv:1605.04320.

[62] N. Palanque-Delabrouille et al., *Constraint on neutrino masses from SDSS-III/BOSS Lyα forest and other cosmological probes*, *JCAP* **1502** (2015), no. 02 045, [arXiv:1410.7244].